



HAL
open science

Chemical extraction of iron from carbonate in banded iron formations for isotope analysis

Eric Siciliano Rego, Vincent Busigny, Pascal Philippot

► **To cite this version:**

Eric Siciliano Rego, Vincent Busigny, Pascal Philippot. Chemical extraction of iron from carbonate in banded iron formations for isotope analysis. *Chemical Geology*, 2022, 611, pp.121120. 10.1016/j.chemgeo.2022.121120 . hal-03784493

HAL Id: hal-03784493

<https://hal.science/hal-03784493>

Submitted on 23 Sep 2022

HAL is a multi-disciplinary open access archive for the deposit and dissemination of scientific research documents, whether they are published or not. The documents may come from teaching and research institutions in France or abroad, or from public or private research centers.

L'archive ouverte pluridisciplinaire **HAL**, est destinée au dépôt et à la diffusion de documents scientifiques de niveau recherche, publiés ou non, émanant des établissements d'enseignement et de recherche français ou étrangers, des laboratoires publics ou privés.

Chemical extraction of iron from carbonate in banded iron formations for isotope analysis

Eric Siciliano Rego^{a, b, *}, Vincent Busigny^c, Pascal Philippot^{b, d}

^a Instituto de Geociências, Universidade de São Paulo, Rua do Lago 562, Cidade Universitária, São Paulo 05508-080, Brazil

^b Géosciences Montpellier, Université de Montpellier, 34095 Montpellier, France

^c Institut de Physique du Globe de Paris, Université Paris Cité, 1 Rue Jussieu, 75238 Paris cedex 05, France

^d Departamento de Geofísica, Instituto de Astronomia, Geofísica e Ciências Atmosféricas, Universidade de São Paulo, Rua do Matão 1226, Cidade Universitária, São Paulo 05508-090, Brazil

ARTICLE INFO

Editor: Dr. Hailiang Dong

Keywords:

Carbonate leachates

Fe isotopes

Acetic acid

Iron formations

ABSTRACT

The iron isotope composition of iron-bearing carbonates is commonly used to obtain insights into ancient environmental conditions. However, it is often challenging to target only Fe-carbonates (e.g. siderite and ankerite) from samples containing a variety of other Fe-bearing minerals, such as observed in Precambrian iron formations. Chemical extraction (i.e. leaching) methods of Fe-carbonates could be an alternative to in-situ measurements and/or micro-drilling techniques applied to isotopic studies. Yet, only a few studies have looked at the effects of leaching carbonates (e.g. partial and/or total dissolution) on their Fe isotope composition. Here, we tested several leaching protocols, using 5 to 20% acetic acid (HAc) and 0.4 M HCl, on a siderite standard and three natural samples, including an iron formation, Fe-rich and Fe-poor carbonates. We showed that carbonate mineralogy has a strong control on how much of each mineral phase was being dissolved, and that variations in HAc concentration from 5% to 20% are less likely to change how much siderite dissolves (e.g. ~30% dissolution) under a 12 h period at room temperature. Importantly, the Fe isotope composition of partially dissolved siderite had indistinguishable values within error from the whole-rock composition (i.e. complete dissolution) as shown with HAc and HCl attacks. Carbonates from the three natural samples were almost completely dissolved under the same protocol with 5 to 20% HAc, while 0.4 M HCl attacks dissolved additional mineralogical phases, which might contribute to the Fe leachate. Moreover, the iron isotope composition of carbonate leachates was preserved without generating anomalous results. Hence, weak chemical leaches represent a reliable tool to study Fe isotopic composition of carbonate to understand how the Fe cycle was operating throughout Earth's history.

1. Introduction

Sedimentary iron-bearing minerals are ancient archives largely used to track changes in the chemical evolution of Earth's oceans through time (Konhauser et al., 2017). There is a general view that iron-bearing carbonates (e.g. siderite and ankerite) and associated iron formations reflect environmental conditions in which they formed, specifically related to anoxic and ferruginous seawater chemistry prior to the Great Oxidation Event (Holland, 2002). Siderite [FeCO₃] and ankerite [Ca(Fe²⁺, Mg, Mn)₂CO₃] represent the dominant and best-preserved carbonate minerals in iron formations (Fe-dolomite and calcite being less common), and have provided key insights into the biogeochemical cycles of iron and carbon throughout Earth's history (Beukes and Klein, 1990; Holland, 1984; James, 1954; Kaufman et al., 1990; Klein, 2005;

Klein and Beukes, 1989; Konhauser et al., 2005, 2017; Raiswell and Canfield, 2012). Significant contributions towards the origin of Fe-carbonates in Precambrian rocks have been made, which rely to some extent in measuring the carbon and iron isotope compositions of these rocks.

Carbon and iron (Fe) isotope signatures are widely used as tools for understanding the processes of Fe-carbonate formation, such as the remineralization of organic matter to produce a depleted ¹³C inorganic carbon source (Beukes et al., 1990; Fischer et al., 2009; Heimann et al., 2010; Johnson et al., 2013), the identification of biological reduction of Fe(III) minerals leading to the enrichment of light Fe isotope (i.e. ⁵⁴Fe) in the reduced Fe phase (Craddock and Dauphas, 2011a; Johnson et al., 2008a; McCoy et al., 2017), and the distinction of kinetic effects associated to mineral precipitation (Jiang et al., 2022; Jiang and Tosca,

* Corresponding author at: Instituto de Geociências, Universidade de São Paulo, Rua do Lago 562, Cidade Universitária, São Paulo 05508-080, Brazil.
E-mail address: ersiciliano@usp.br (E.S. Rego).

2019). Carbon isotope composition in carbonates is easily measured in iron formations through gas extraction via reaction of whole-rock powders with orthophosphoric acid (Becker and Clayton, 1972; Busigny et al., 2013; Fischer et al., 2009; Garcia et al., 2021; Kaufman et al., 1991; Lebeau et al., 2014). In contrast, the analysis of Fe isotope composition of distinct Fe-mineral phases such as carbonates, as well as oxides (e.g. magnetite, hematite), sulfides (e.g. locally pyrites), and minor phyllosilicates (e.g. stilpnomelane, riebeckite), is often more challenging. Previous studies have tackled this issue using micro-drilling techniques (Heimann et al., 2010), in-situ analysis (Marin-Carbonne et al., 2020; Steinhofel et al., 2010), and chemical leaching procedures to target distinct minerals (Frost et al., 2007; Hyslop et al., 2008; von Blanckenburg et al., 2008). In the case of carbonates, this might be difficult using only micro-drilling techniques, particularly in IFs, where siderite and/or ankerite can be disseminated in chert matrixes closely associated and surrounded by Fe-oxides with varying sizes (e.g. nm to cm) (e.g. Kaufman et al., 1990).

A simple method used for isotope analysis of carbonates is weak acetic acid extractions, as illustrated for Sr isotopes measurement (Bayon et al., 2002). However, only a few studies have reported the effect of leaching carbonates on their Fe isotope composition (Hyslop et al., 2008; von Blanckenburg et al., 2008). Therefore, it is not clear if acetic acid can be efficiently applied for Fe isotope analysis of Fe-bearing carbonates. Importantly, when targeting only carbonates, all of the other mineral phases should be avoided. The sequential extraction of Fe-carbonates with sodium acetate has shown to be an efficient technique dissolving completely the carbonates contained in sediments (PC method; Poulton and Canfield, 2005; Oonk et al., 2017). However, the PC method has also proven to be challenging particularly in carbonates exposed to higher metamorphic grades (Slotznick et al., 2018), although no Fe isotopic work has been done examining specifically the Fe speciation proxy in Precambrian rocks (only modern sediments were studied; Henkel et al., 2016). The present contribution aims at filling this gap by testing the effect of a simple weak acetic acid leaching protocol on iron isotope fractionation in a siderite standard and three natural rock samples. The selected natural samples contain various mixtures of Fe minerals with different shapes and sizes, and include one Precambrian iron formation (Fe-oxide facies), as well as one Fe-rich and one Fe-poor carbonate. The protocols are shown to be reproducible, reliable and accurate, and can therefore be used as a tool for targeting carbonates in the ancient rock record without significantly dissolving other minerals. More importantly, this method provides a means to identify Fe isotope signatures that could be masked when utilizing other mineral separation and/or dissolution methods.

2. Samples and method

The three samples analyzed in this study comprise an iron formation, and Fe-rich and Fe-poor carbonates from the 2.7 Ga-old Carajás Formation, Brazil, and were recently described in Rego et al. (2021). Additionally, a siderite powder (SID) from the deposits of La Mûre, France (Lebeau et al., 2014), was selected for our experiments. International geostandards used uniquely for Fe isotopic measurements includes BCR-2 (basalt, Columbia River, Oregon, USA – USGS), BHVO-2 (basalt, Kilauea, Hawaii, USA – USGS), AC-E (granite, Ailsa Craig Island, Scotland – SARM), IF-G (iron formation, Isua, Greenland – SARM), and an internal Fe standard referred to as ISVB (Institut de Physique du Globe de Paris - IPGP, France). All of the following procedures and measurements were performed at IPGP.

2.1. Leaching protocol

Approximately 40 mg of whole rock powder of iron formation (FD-55463), Fe-rich (FD-55521) and Fe-poor carbonates (FD-55478) were digested in a pre-cleaned 15 ml polypropylene tube by adding 3 ml of

ultra-pure acetic acid (HAc) with different concentrations (5%, 10%, and 20% v/v). In parallel, the procedure was also performed using 0.4 M HCl (Fig. 1). All the samples were left overnight at room temperature (12h), and centrifuged (6 min/5000 rpm) the next day. The clear supernatant was then transferred into acid-cleaned Savillex Teflon beakers, while the residues were washed three times with MilliQ H₂O, dried, and weighed to record any mass loss after digestion. The supernatant was evaporated, and subsequently digested with concentrated HNO₃ and HCl (2:1 volume ratio) and heated overnight at 100 °C. Samples were evaporated the next day and were brought back into solution in 6 M HCl. The same complete procedure was applied to the siderite standard (SID), but only 4 mg of SID powder was used and digested in 3 ml of 5%, 10%, and 20% HAc, and in 5 ml of HCl 0.4 M. At least two replicates were made for each treated sample.

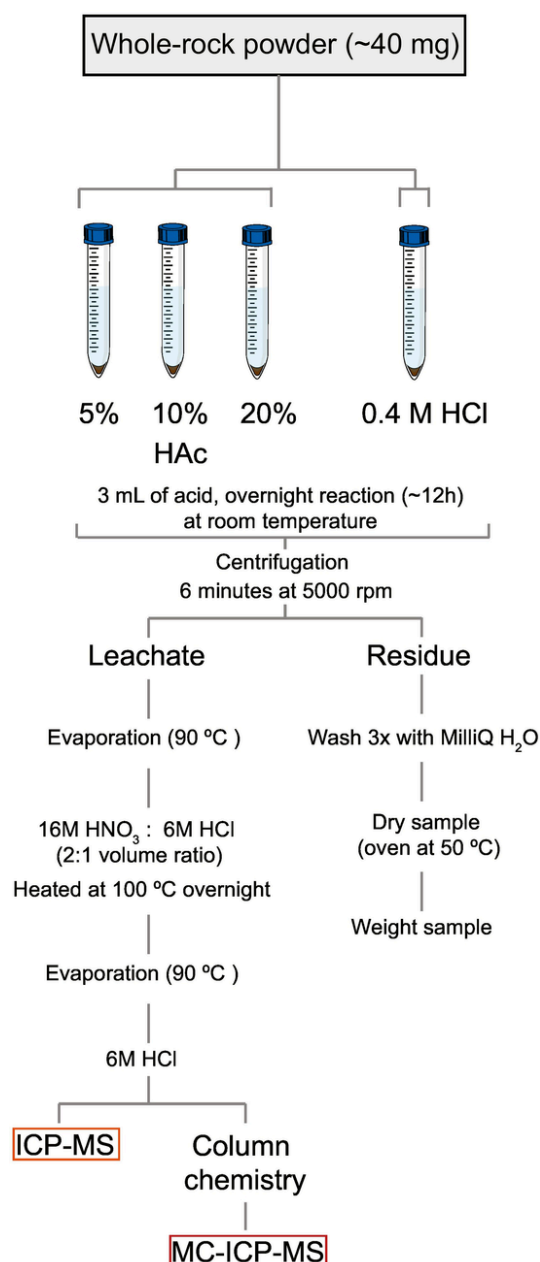


Fig. 1. Chemical leaching protocol utilized in this study.

2.2. Iron isotope analysis

Iron isotopic compositions were measured on the leachate fraction (see above) and on whole rock samples, including the siderite SID and international geostandards. In the case of whole rock measurements, approximately 10 to 20 mg of rock powder were dissolved with concentrated mixtures of HF, HCl, HNO₃ to ensure complete digestion and that all iron was in its ferric state.

All samples were dissolved in 6 M HCl prior to iron column chemistry. Iron was purified twice through anion exchange chromatography following an adaptation from Dauphas et al. (2004, 2009) which has been described in previous studies (e.g. Busigny et al., 2014, 2017, 2018). In brief, Bio-Rad Poly-Prep columns were filled with 1 ml anion exchange resin (AG1-X8 200–400 mesh chloride form). The resin was cleaned three times with 10 ml H₂O and 5 ml 1 M HNO₃. It was then preconditioned in HCl medium by running 10 ml H₂O, 10 ml 0.4 M HCl, 5 ml H₂O and 2 ml 6 M HCl. Matrix elements were eluted in 8 ml 6 M HCl, whereas Fe(III) was strongly adsorbed on the resin and quantitatively retained. Iron was subsequently eluted in 10 ml 0.4 M HCl.

Iron isotope compositions were measured using a ThermoFischer Neptune MC-ICP-MS (Multiple Collector Inductively Coupled Plasma Mass Spectrometer) at the Institut de Physique du Globe de Paris (IPGP). The samples were introduced into the mass spectrometer with a quartz cyclonic spray chamber and analyzed in 0.3 M HNO₃ at a concentration of ~2–3 ppm, which gave a signal of ~16 to 20 V on ⁵⁶Fe. The isotopes ⁵⁴Fe⁺, ⁵⁶Fe⁺, ⁵⁷Fe⁺ and ⁵⁸Fe⁺ were measured simultaneously, while ⁵³Cr⁺ and ⁶⁰Ni⁺ were also measured to monitor and correct any contribution on ⁵⁴Fe⁺ and ⁵⁸Fe⁺, respectively. Faraday cups were collecting masses 53, 54, 56, 57, 58, and 60 in Low 3, Low 2, High 1, High 2, and High 4, respectively. Iron isotopes were fully resolved from argide interferences (⁴⁰Ar¹⁴N⁺, ⁴⁰Ar¹⁶O⁺, ⁴⁰Ar¹⁶O¹H⁺) using the high-resolution mode of the Neptune (Weyer and Schwiders, 2003). Instrumental mass discrimination was corrected using the conventional sample-standard bracketing (SSB) approach (Rouxel et al., 2003). The ⁵⁶Fe/⁵⁴Fe and ⁵⁷Fe/⁵⁴Fe ratios were expressed in the usual δ notation in per mil (‰) as,

$$\delta^{56}\text{Fe} (\text{‰}) = \left[\left(\frac{{}^{56}\text{Fe}/{}^{54}\text{Fe}}{\text{sample}} / \left(\frac{{}^{56}\text{Fe}/{}^{54}\text{Fe}}{\text{standard}} - 1 \right) \right) \times 1000 \right]$$

$$\delta^{57}\text{Fe} (\text{‰}) = \left[\left(\frac{{}^{57}\text{Fe}/{}^{54}\text{Fe}}{\text{sample}} / \left(\frac{{}^{57}\text{Fe}/{}^{54}\text{Fe}}{\text{standard}} - 1 \right) \right) \times 1000 \right]$$

where the standard is IRMM-014, a pure synthetic Fe metal from the Institute for Reference Materials and Measurements (Taylor et al., 1992). The Fe blank level of the present procedure has been evaluated by systematic analyses of one blank in each sample series, prepared as described above but without any sample powder. The blank was always below 20 ng Fe, thus representing < 0.3% of the total Fe measured in sample solutions.

Accuracy and analytical precision were determined by measuring international rock geostandards AC-E, BCR-2, BHVO-2, and IF-G as shown in Table 1, while long-term ⁵⁶Fe/⁵⁴Fe, ⁵⁷Fe/⁵⁴Fe, and ⁵⁷Fe/⁵⁶Fe mea-

Table 1
Measured iron isotopic composition of international geostandards.

Standard	⁵⁶ Fe (‰) ^a	± 2SD ^b	⁵⁷ Fe (‰) ^a	± 2SD ^b
AC-E	0.324	0.006	0.505	0.052
	0.310	0.044	0.483	0.080
	0.323	0.016	0.497	0.052
BCR-2	0.071	0.028	0.116	0.056
BHVO-2	0.107	0.020	0.145	0.048
	0.103	0.042	0.178	0.052
IF-G	0.613	0.021	0.895	0.076
(n = 12)				

surements of IF-G and the internal standard ISVB are shown in Fig. 2. The Fe isotopic compositions of the geostandards had external precision and accuracy always better than 0.046 ‰ for ⁵⁶Fe and 0.08 ‰ for ⁵⁷Fe (2SD) and were in good agreement with recommended values (Craddock and Dauphas, 2011b).

2.3. Iron concentration

Iron concentrations were obtained using an Agilent 7900 quadrupole ICP-MS at IPGP. Measurements were done using a collision-reaction cell with helium gas (5 ml/min) to remove polyatomic interferences. A scandium internal-standard was injected after inline mixing with the samples to correct for signal drift and matrix effects. A set of iron calibration standards was analyzed to confirm and model (through simple linear regression) the linear relationship between signal and concentration. The model was then used to convert measured sample counts concentrations. Reported uncertainties were calculated using error propagation equations and considering the combination of standard deviation on replicated consecutive signal acquisitions (n = 3), internal-standard ratio and blank subtraction. The non-linear term (internal-standard ratio) was linearized using a first-order Taylor series expansion to simplify error propagation.

2.4. Mineralogy

Mineralogical characterization was determined from thin sections observation by reflected and transmitted light microscopy at the Université de Montpellier. This was complemented by scanning electron microscopy (SEM) and energy-dispersive X-ray spectroscopy (EDS) on carbon-coated samples, utilizing a Zeiss EVO MA10 SEM for semi-quantitative SEM-EDS analysis at the Institut de Physique du Globe de Paris (IPGP). Standard operating conditions for SEM imaging and EDS analysis were 15 kV accelerating voltage, working distance of 12 mm, and 2–3 nA electron beam current (see detailed conditions in Rego et al., 2021).

2.5. Carbonate content

Approximately 40 mg, 10 mg, and 5 mg of sample powder was used for IF, Fe-rich, and Fe-poor carbonates, respectively. The powder was loaded in Labco Exetainer® sample vials, flushed with helium and treated with 100% phosphoric acid at 130 °C for 2 h to dissolve all carbonates, including siderite (Busigny et al., 2013; Lebeau et al., 2014; Rosenbaum and Sheppard, 1986). The produced CO₂ was measured using a continuous-flow mass-spectrometer (AP-2003) operated with helium as a carrier gas (Lebeau et al., 2014). Carbonate content in samples was estimated from the ion intensity of the CO₂ peak in the mass-spectrometer with a precision better than ± 10% (2SD).

2.6. Magnetite separation

In order to test if acetic acid treatments dissolves, even partially, magnetite, a mineral commonly present with carbonates in Precambrian sediments, we separated ~10 mg of magnetite grains from two samples, including an iron formation and an Fe-carbonate (Fig. 3). Magnetite was separated from whole-rock powders by utilizing a neodymium-iron-boron magnet (disc magnet with a diameter of 5 mm and a height of 5 mm). Whole-rock samples were washed in a pre-cleaned 15 ml polypropylene tubes at least 10 times using MilliQ H₂O and magnetite was removed simultaneously with an aid from the magnet. The non-magnetic fraction was discarded and the sample was washed until all the magnetic fraction was separated. After washing, the magnetic fraction was dried in an oven at 50 °C overnight. The following day, the same leaching protocol described previously (5%, 10%, 20% HAc; 12 h reaction, room temperature; see section 2.1) was ap-

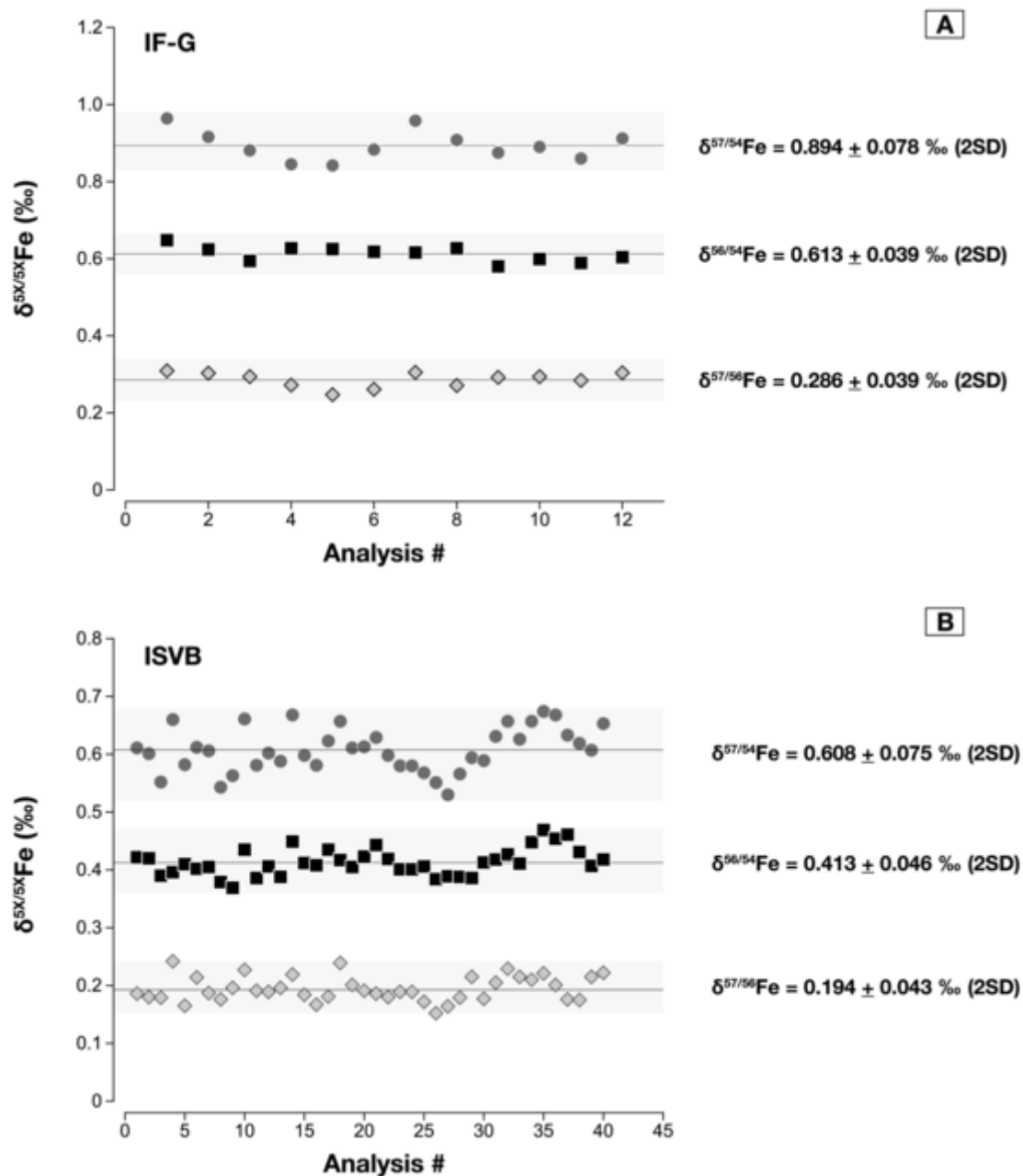


Fig. 2. Long-term measurements of the iron isotope compositions of IF-G geostandard and ISVB (internal Fe standard).

plied to the magnetite grains. The dissolution was monitored by measuring Fe concentration by ICP-MS in the supernatant solution after the leaching treatment.

3. Results

As explained above, weak acid leaching protocols were tested on a siderite (FeCO_3) standard (Lebeau et al., 2014) and in Neoproterozoic (~2.74 Ga) iron formation and carbonate samples from Carajás, Brazil (Rego et al., 2021). The results of the leaching experiments and whole rock sample dissolution are reported in Tables 2 and 3. It includes sample's mass loss (wt%) after each treatment, whole-rock carbonate content (%) determined from CO_2 extraction and measurement, the fraction of Fe-carbonate dissolved (%) calculated based on the Fe concentration in solution after leaching treatments (i.e. assuming that ankerite was the dissolved Fe-carbonate phase for all Neoproterozoic samples), and Fe isotope compositions of various leachates or bulk powder dissolu-

tions. Additionally, acetic acid (HAc) leaching protocol was also performed on pure magnetite grains to identify any dissolution, which could bring a potential source of contamination to the carbonate fraction leached from natural samples (Table 4).

3.1. Siderite standard

The siderite standard was leached with three distinct HAc concentrations (i.e. 5%, 10%, and 20% HAc) for 12 h (h) at room temperature. When treated with 5% HAc, the mass loss ranged from 27.7 to 31.6 wt% (average of $29.7 \pm 2.69\%$, $n = 2$) while treatments with 10 and 20% HAc induced a mass loss between 22.2 and 37.1 wt% (average of $29.65 \pm 10.54\%$, $n = 2$), and 33.3 to 59.3 wt% (average of $46.3 \pm 18.38\%$, $n = 2$), respectively (Table 2). Specifically, one sample treated with 20% HAc had significantly larger mass loss (i.e. 59.3 wt%) when compared to all other samples (Table 2). The average dissolved Fe-carbonate content for our siderite standard ($\text{Fe-carb}_{\text{siderite}}$)

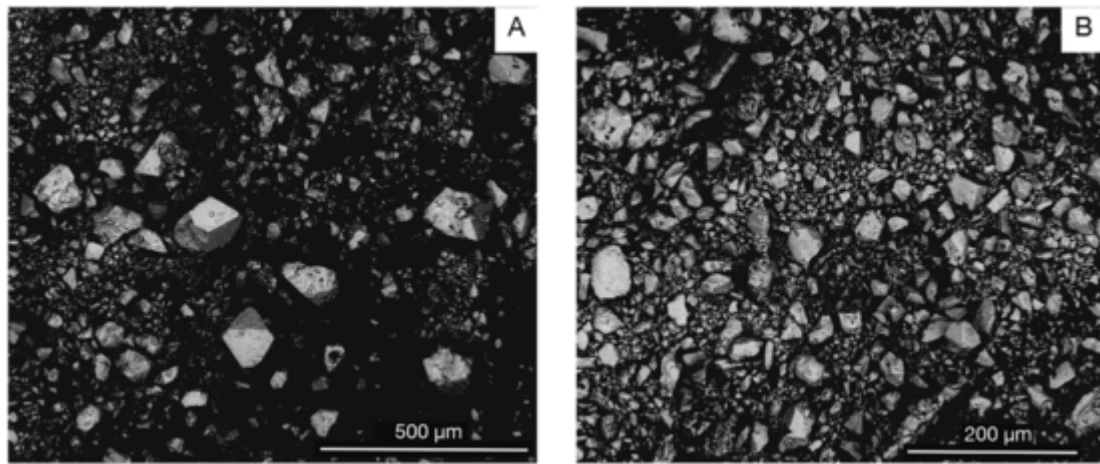


Fig. 3. Magnetite grains of varying sizes removed from (A) an iron formation sample and from (B) Fe-rich carbonate sample.

Table 2

Results of various leaching protocols showing changes in mass loss, Fe dissolved in leachate, and iron isotopic compositions of the leachate fraction for specific carbonate phases. Literature data are added when available.

Acid treatments	Samples	Time (h)	Temp. (°C) ^a	Mass loss (wt%) ^b	Fe-carbonate dissolved in leachate (%) ^c	$\delta^{56}\text{Fe}$ (‰) ^d	$\pm 2\text{SD}^e$	$\delta^{57}\text{Fe}$ (‰) ^d	$\pm 2\text{SD}^e$	References
5% HAc	Siderite (SID)	12	20–21	31.6	13.5	−0.29	0.02	−0.44	0.03	This study
5% HAc	Siderite (SID)	12	20–21	27.8	34.4	−0.30	0.02	−0.46	0.03	This study
10% HAc	Siderite (SID)	12	20–21	22.2	34.0	−0.30	0.04	−0.48	0.06	This study
10% HAc	Siderite (SID)	12	20–21	37.1	20.6	−0.33	0.02	−0.53	0.03	This study
10% HAc	Dolomite	12	20–21		34.2					von Blanckenburg et al., 2008
10% HAc	Stromatolitic calcite LN-01	12	20–21		54.7					von Blanckenburg et al., 2008
10% HAc	Stromatolitic calcite BL-1	12	20–21		68.9					von Blanckenburg et al., 2008
10% HAc	Ankerite	12	20–21		93.6					von Blanckenburg et al., 2008
20% HAc	Siderite (SID)	12	20–21	33.3	25.8	−0.33	0.03	−0.50	0.04	This study
20% HAc	Siderite (SID)	12	20–21	59.3	36.8	−0.30	0.01	−0.46	0.02	This study
20% HAc	Siderite powder	24	40		61.5					Hyslop et al., 2008
0.4 M HCl	Siderite (SID)	96	20–21		101.81	−0.31	0.08	−0.49	0.18	This study
0.4 M HCl	Siderite (SID)	96	20–21		95.45	−0.35	0.05	−0.48	0.28	This study
0.4 M HCl	Siderite (SID)	96	20–21		80.06	−0.29	0.08	−0.42	0.09	This study
0.75 M HCl	Siderite powder	43	20–21		99.6					Hyslop et al., 2008
Whole rock/complete dissolution	Siderite (SID)					−0.31	0.08	−0.45	0.14	This study
Whole rock/complete dissolution	Siderite (SID)					−0.34	0.03	−0.53	0.10	This study

^a Temperatures between 20 and 21 °C are considered room temperature.

^b Mass loss weight percent calculated by weighting the residue after leaching protocol.

^c The amount of Fe-carbonate (i.e. siderite) dissolved calculated relative to the Fe content in the leachate solution. Fe concentrations were measured by ICP-MS.

^d Iron isotopic ($\delta^{56}\text{Fe}$ and $\delta^{57}\text{Fe}$) ratios are reported in per mil difference relative to iron metal standard IRMM-014.

^e Analytical errors are reported as 2 standard-deviation (2SD).

was calculated based on the amount of Fe measured in the leachate fraction after HAc treatments. The values were $23.95 \pm 14.78\%$ Fe-carbonate_{siderite} dissolved for 5% HAc ($n = 2$), $27.30 \pm 9.48\%$ ($n = 2$), and $31.30 \pm 7.78\%$ Fe-carbonate_{siderite} dissolved ($n = 2$) for 10% and 20% HAc, respectively. A similar protocol was implemented utilizing 5 ml of 0.4 M HCl to leach the same siderite powder. All three replicates were almost completely digested with 80.6 to 101.81% of dissolved siderite after a 96 h treatment at room temperature (Table 2).

The average $\delta^{56}\text{Fe}$ value for the whole rock siderite standard was -0.33 ± 0.02 ‰ ($n = 2$), indistinguishable from the leaching with 5%, 10%, and 20% HAc, after 12 h reaction time at room temperature (-0.30 ± 0.01 ‰ ($n = 2$), -0.31 ± 0.02 ‰ ($n = 2$), and -0.31 ± 0.02 ‰ ($n = 2$), respectively). Moreover, siderite samples leached with 0.4 M HCl after a 96 h reaction time at room temperature, had an average $\delta^{56}\text{Fe}$ value of -0.32 ± 0.03 ‰ ($n = 3$) (Fig. 4).

3.2. Iron formation and carbonates

The studied samples consisting of IF, Fe-rich and Fe-poor carbonates from Carajás basin have been previously described in Rego et al. (2021) and the mineralogical assemblages were similar to those shown by Justo et al. (2020). Carbonates in IF facies in Carajás occur commonly as ankerite $[\text{Ca}(\text{Fe}^{2+}, \text{Mg}, \text{Mn})\text{CO}_3]$ disseminated in a microcrystalline quartz (chert) matrix (Fig. 5A,B). Other Fe-mineral phases in IF include abundant euhedral magnetite crystals, microscopic spheroidal hematite, minor Fe-silicates, and very few pyrites (Rego et al., 2021). Iron-rich and iron-poor carbonate rock samples show higher carbonate content, but differ from each other particularly by the occurrence of calcite $[\text{CaCO}_3]$ and framboidal pyrites $[\text{FeS}_2]$ within Fe-poor facies (Figs. 5C and 3.8).

Table 3

Variations in mass loss, amount of Fe dissolved, and iron isotopic compositions for different acid leachates using rock matrix (IF, Fe-rich, and Fe-poor carbonates), including carbonate content measured on whole-rock.

Sample	Lithology	Acid treatment	Mass loss (wt%)	Fe-carbonate dissolved in leachate (%) ^a	Carbonate (calcite %) ^b	Carbonate (ankerite %) ^b	Carbonate (siderite %) ^b	$\delta^{56}\text{Fe}$ (‰) ^c	$\pm 2\text{SD}^d$	$\delta^{57}\text{Fe}$ (‰) ^c	$\pm 2\text{SD}^d$
FD55 463.52	IFs	5% HAC	18.4	9.72	9.34	9.41	10.83	0.14	0.04	0.23	0.06
		5% HAC	13.6	8.48	9.44	9.52	10.96	0.15	0.08	0.22	0.09
		10% HAC	13.0	6.56				0.14	0.04	0.16	0.06
		10% HAC	18.0	6.80				0.17	0.06	0.23	0.07
		20% HAC	12.9	5.60				0.12	0.06	0.18	0.09
		20% HAC	13.8	6.83				0.14	0.06	0.20	0.12
		0.4 M HCl	38.2					0.20	0.05	0.31	0.08
FD55 521.63	Fe-rich carb.	5% HAC	28.5	26.88	25.12	25.32	29.14	-0.74	0.06	-1.12	0.06
		5% HAC	28.2	48.31	24.71	24.91	28.67	-0.73	0.07	-1.10	0.08
		10% HAC	27.2	35.78				-0.70	0.03	-1.06	0.08
		10% HAC	27.7	39.33				-0.70	0.04	-1.05	0.06
		20% HAC	29.1	36.65				-0.73	0.04	-1.06	0.07
		20% HAC	27.4	35.87				-0.71	0.05	-1.06	0.11
		0.4 M HCl	32.9					-0.67	0.06	-1.00	0.08
FD55 478.03	Fe-poor carb.	5% HAC	55.3	35.69	61.81	62.30	71.70	-0.15	0.05	-0.22	0.07
		5% HAC	56.7	41.80	51.54	51.82	59.63	-0.16	0.07	-0.20	0.10
		10% HAC	58.0	39.34				-0.16	0.02	-0.29	0.03
		10% HAC	59.0	46.82				-0.14	0.02	-0.20	0.05
		20% HAC	60.1	43.97				-0.14	0.03	-0.23	0.07
		20% HAC	58.6	45.22				-0.17	0.07	-0.26	0.11
		0.4 M HCl	54.8					-0.19	0.06	-0.27	0.10
		0.4 M HCl	64.3					-0.19	0.04	-0.27	0.07

^a The amount of Fe-carbonate (i.e. ankerite) dissolved calculated relative to the Fe content in the leachate solution. Fe concentrations were measured by ICP-MS.

^b Carbonate content measured on whole-rock in AP-2003 after reaction with 100% orthophosphoric (2 h at 130 °C). Relative error of ± 10 wt% established after measuring siderite standard (average = 103.3 ± 9.5 wt%, 1sd, $n = 3$).

^c Iron isotopic ($\delta^{56}\text{Fe}$ and $\delta^{57}\text{Fe}$) ratios are reported in per mil difference relative to iron metal standard IRMM-014.

^d Analytical errors are reported as 2 standard-deviation (2SD).

Table 4

Magnetite dissolution tests with 5% and 10% acetic acid (HAc).

Sample	Treatment	Weight (mg) ^a	Fe in leachate (%) ^b
Magnetite 1	5% HAC, 25 °C, 12 h	11.2	0.04
Magnetite 2	5% HAC, 25 °C, 12 h	7.1	0.003
Magnetite 3	10% HAC, 25 °C, 12 h	9.1	0.08

^a weight of sample loaded for magnetite dissolution experiment (acetic acid volume was 5 mL).

^b Fe in leachate corresponds to the fraction of Fe expressed relative to total Fe (calculated from the magnetite mass and assuming a pure Fe_3O_4).

In order to target only carbonate phases, we applied the same leaching protocol (i.e. 5%, 10% and 20% HAC and 0.4 M HCl) among three distinct samples, including an IF (FD 55–463.55), Fe-rich (FD 55–521.63) and Fe-poor (FD 55–478.03) carbonate sample. The average mass loss after HAC treatment (5%, 10%, and 20% HAC, 12 h, room temperature) for the IF sample was 14.95 ± 2.5 wt% ($n = 6$), while Fe-rich and Fe-poor carbonate samples lost 28.02 ± 0.7 wt% ($n = 6$) and 57.95 ± 1.7 wt% ($n = 6$) of their masses, respectively (Table 3). The amount of Fe-carbonate dissolved after HAC treatment, here considering that carbonates were ankerite (Fe-carbonate_{ankerite}), was lower for the IF sample, ranging from 5.60 to 9.72% (average of $7.3 \pm 1.5\%$ $n = 6$), and higher for Fe-rich and Fe-poor carbonates, varying between 26.88 and 48.31% (average of $37.1 \pm 6.9\%$, $n = 6$), and 35.69 to 46.82% (average of $42.1 \pm 4.1\%$, $n = 6$), respectively. Additionally, samples treated with 0.4 M HCl with the same experimental conditions (12 h at room temperature) showed higher mass loss, particularly the IF sample. Iron formation and Fe-rich carbonate samples lost 38.2 wt% and 32.9 wt% of their masses, respectively, while Fe-poor carbonate sample lost up to 64.3 wt% of its mass (Table 3). The carbonate content estimated from CO_2 measurements of IFs and Fe-rich carbonates was

$9.5 \pm 0.08\%$ (average, $n = 2$) and $25.12 \pm 0.29\%$ (average, $n = 2$), respectively. These values were calculated by assuming that ankerite [$\text{Ca}(\text{Fe}^{2+}, \text{Mg}, \text{Mn})\text{CO}_3$] is the dominant carbonate phase in those samples. In Fe-poor carbonates, calcite content increases, and carbonate estimates based on CO_2 extraction averages $56.68 \pm 7.26\%$ CaCO_3 ($n = 2$).

The iron isotope composition of IF leachates treated with 5%, 10%, and 20% HAC varied between $+0.12$ ‰ to $+0.17$ ‰ with an average of $+0.14 \pm 0.02$ ‰ ($n = 6$), slightly lighter compared to 0.4 M HCl treatment that showed a $\delta^{56}\text{Fe}$ value of $+0.20 \pm 0.05$ ‰ (Table 3, Fig. 7). Iron-rich carbonate leached with HAC displayed $\delta^{56}\text{Fe}$ values averaging -0.72 ± 0.02 ‰ ($n = 6$), again slightly lighter compared to the HCl treatment (i.e. $\delta^{56}\text{Fe}$ value of -0.67 ± 0.06 ‰). In contrast, the iron-poor carbonate sample had moderately heavier iron isotopic composition for HAC leachates (e.g. average $\delta^{56}\text{Fe}$ value of -0.15 ± 0.01 ‰, $n = 6$) compared to the HCl leachate (e.g. $\delta^{56}\text{Fe} = -0.19 \pm 0.01$ ‰, $n = 2$, Table 3, Fig. 7).

3.3. Magnetite dissolution

Magnetite grains treated with 5% and 10% HAC at room temperature for 12 h showed a negligible fraction of Fe in their leachate solution, ranging from 0.003% to 0.08% of Fe with an average of $0.04 \pm 0.04\%$ Fe ($n = 3$) after both treatments (Table 4).

4. Discussion

4.1. Partial dissolution of Fe-carbonate standard but preservation of its Fe isotope composition

We tested the acetic acid leaching protocol on a siderite (FeCO_3) standard (Lebeau et al., 2014) with the aim of (i) estimating how much

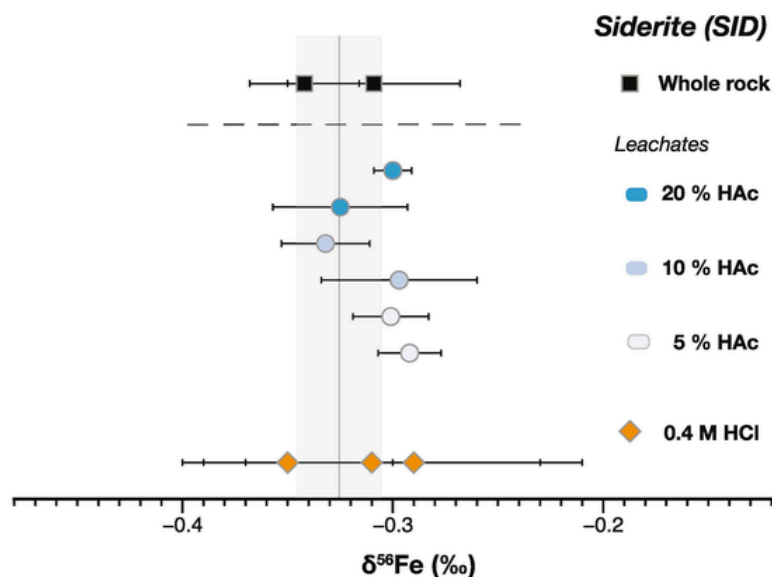


Fig. 4. Iron isotope ($\delta^{56}\text{Fe}$) composition of whole-rock siderite and leachates utilizing acetic acid (HAc) of different concentrations (5 to 20%) and 0.4 M HCl. Error bars represent analytical errors reported as 2 standard-deviation.

of the carbonate is being dissolved and (ii) determining if the Fe isotope composition of the dissolved fraction is representative of its whole rock composition. There was no significant mass loss variation (22.2 wt% to 37.1 wt%) for acid digestions with distinct HAc concentrations (Table 2). Although a single sample lost 59.3 wt% of its mass when treated with 20% HAc, this may be due to mass loss while washing, drying and weighing the sample (i.e. not related to siderite dissolution). Specifically, the amount of Fe-carbonate_{siderite} dissolved, as calculated relative to the Fe concentration in the leachate fraction for this sample, was not significantly different from other samples. All HAc treatments (e.g. 5%, 10%, and 20% HAc) yielded an average of $27.51 \pm 9.2\%$ ($n = 6$) of Fe-carbonate_{siderite} dissolved in the leachate (Table 2), suggesting a partial digestion of siderite for all treatments. This is in agreement with previous estimates that performed similar tests (e.g. 10% HAc digestion, 12 h period, room temperature) in dolomitic carbonate (34.2% Fe dissolved), however lower than expected when compared to Fe dissolved in stromatolitic calcite (57.4%) and ankerite (93.6%) (von Blanckenburg et al., 2008) (see literature data also compiled in Table 2). Interestingly, Hyslop et al. (2008) reported that siderite dissolution during longer time (24 h) and at higher temperature (40 °C) was also partial (61.5%) (Table 2). Altogether, the present and previous results indicate that carbonate mineralogy (composition, structure, grain size, porosity) has a strong control on how much of each mineral phase is being dissolved, and that variations in HAc concentration from 5% to 20% are less likely to change how much siderite is being dissolved under a 12 h period at room temperature.

Other dissolution techniques, such as the utilization of sodium (Na) acetate to target Fe-carbonates from modern and ancient sediments, have shown to dissolve ~100% of the Fe-carbonate phase in the sample (Poulton and Canfield, 2005). Only few studies have adapted this sequential extraction protocol with an aim to measure the Fe isotope composition of different Fe-phases in modern and Phanerozoic sediments (Havas et al., 2021; Henkel et al., 2016). Despite showing a good extraction efficiency for Fe-carbonates, the Na-acetate method is significantly longer and cumbersome (e.g. adjusting pH, removing Na-acetate prior to Fe chromatography, etc.) compared with the proposed protocol. Therefore, identifying other efficient carbonate leaching techniques, such as weak HAc and HCl digestions, could be advantageous and suitable for Fe isotopic studies.

Even though our results supports previous findings that diluted HAc does not achieve complete dissolution of siderite (e.g.

Rongemaille et al., 2011), the remaining question is whether partial dissolution of siderite, as opposed to near complete dissolution (see Table 2), could still preserve the Fe isotopic composition of the bulk siderite. Given that a fraction of ~30% of Fe-carbonate was dissolved with different HAc concentrations, we show that the iron isotopic composition of the leachates (-0.30 ± 0.01 ‰ for 5% HAc; -0.31 ± 0.02 ‰ for 10% HAc; and -0.31 ± 0.02 ‰ for 20% HAc) had undistinguishable values within error from the whole-rock composition (-0.33 ± 0.02 ‰, $n = 2$) (Fig. 4). Moreover, there is also no significant difference in Fe isotope composition between different acid treatments (Fig. 4). This shows that HAc (5%, 10% and 20%) and 0.4 M HCl are capable of leaching siderite and still preserve its Fe isotopic composition despite partial or almost complete dissolution of the Fe-carbonate phase. The lack of fractionation observed between the partially dissolved and completely dissolved siderite is expected given that there was no exchange between other Fe mineral phases. This is in contrast with previous studies that leached granite and basalts and recorded fractionation between fluids and solids (e.g. kinetic effects associated to light isotopes being preferentially leached over the heavy isotopes, Chapman et al., 2009; (Nie et al., 2020)) If any fractionation occurred between fluid and solid phase this was likely small and could not be resolved within analytical uncertainty. Finally, this will have implications particularly when applying the leaching protocol to powders from complex rock matrixes, in which the presence of other mineralogical phases (e.g. Fe-oxides, phyllosilicates) might challenge the precise targeting of carbonates.

4.2. Reliable iron isotope measurements of carbonates in natural samples from acetic acid leaching

In order to evaluate complete and/or partial carbonate dissolution in typical Archean samples, such as IF, Fe-rich and Fe-poor carbonates, we examine the results of three independent methods, and compare (i) carbonate content measured on whole-rock powders from CO₂ extraction with (ii) changes in mass loss determined after HAc leaching, and with (iii) the amount of Fe-carbonate estimated from Fe concentrations obtained in the leachate fraction (Table 3). The IF sample had a carbonate content of $9.5 \pm 0.08\%$ ($n = 2$) calculated for ankerite based on its whole-rock composition, and had a similar amount of Fe-carbonate_{ankerite} determined from Fe in the leachate (e.g. average of $7.33 \pm 1.5\%$, $n = 6$). This implies that most of the Fe-carbonates, pre-

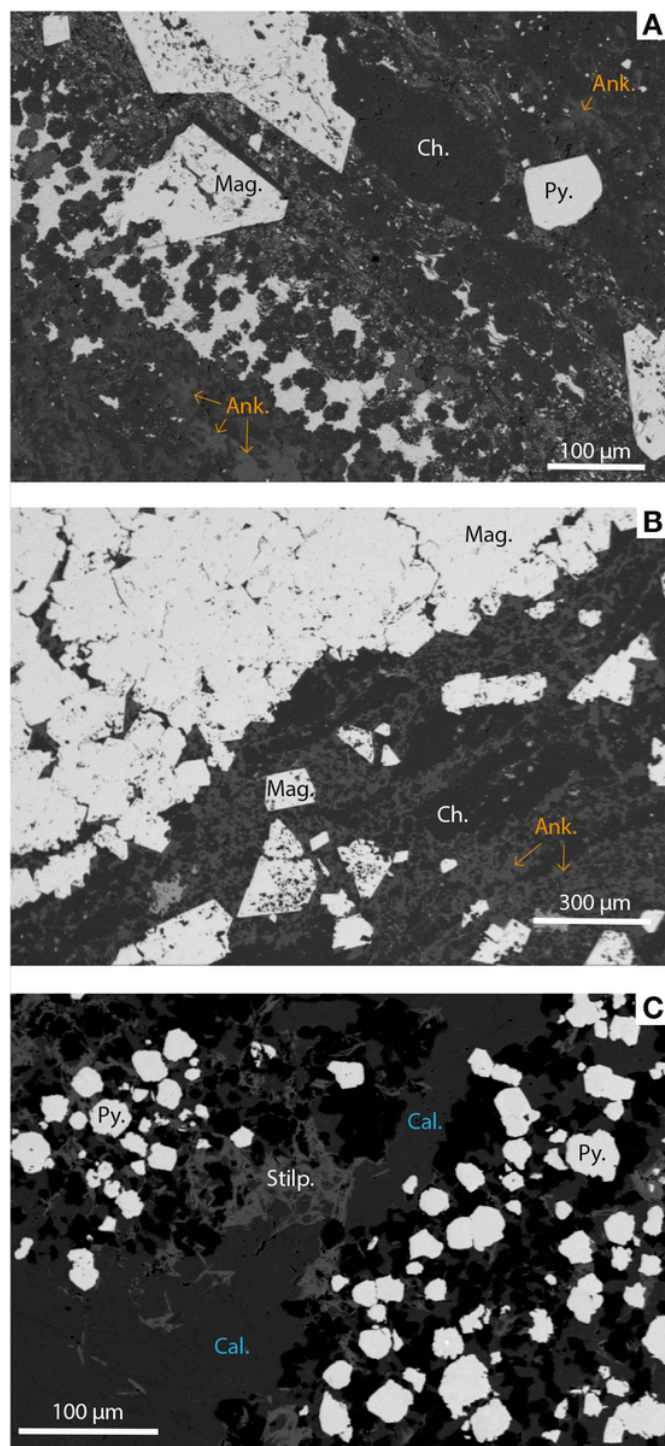


Fig. 5. Petrographic context of an (A) iron formation, (B) Fe-rich, and (C) Fe-poor carbonate samples showing ankerite disseminated in a chert matrix surrounded by magnetite grains (A and B), while calcite is more abundant in the Fe-poor sample also containing framboidal pyrites (C).

dominantly ankerite as shown by petrographic work (Figs. 5 and 6) (Justo et al., 2020; Rego et al., 2021), were dissolved. The average mass loss of 14.95 ± 2.5 wt% ($n = 6$) after HAC treatments was slightly higher when compared to the carbonate content and Fe-carbonate_{ankerite} dissolution estimates. This difference may reflect additional dissolution of another phase (containing no Fe) and/or a systematic error associated to the mass loss estimate (e.g. by weighing the sample before treatment, weighing empty tubes, weighing samples after treatment, wash-

ing and removing solution after centrifugation, etc.). The relative uncertainty on carbonate content determination from mass loss may be high particularly in this sample because of its low carbonate content compare to other samples.

Iron-rich carbonate sample has a higher carbonate content of $25.12 \pm 0.29\%$ ($n = 2$) as determined from CO_2 production, close to the value of 28.02 ± 0.7 wt% ($n = 6$) estimated from its mass loss after HAC treatment (Table 3). This suggests again that most carbonates were dissolved after HAC treatment. However, the average fraction of dissolved Fe-carbonate_{ankerite} calculated based on the Fe concentration in the leachate was significantly higher, with a value of $37.14 \pm 6.9\%$ ($n = 6$).

This difference possibly results from the dissolution an additional Fe-bearing phase during acid treatments. Comparably, the HAC treatments dissolved all carbonates in the Fe-poor carbonate sample, as shown by indistinguishable values in measured carbonate content (e.g. $56.68 \pm 7.26\%$, $n = 2$) and mass loss values (e.g. 57.95 ± 1.7 wt%, $n = 6$). Given that the Fe-poor carbonate sample contains a large amount of calcite in addition to ankerite (Figs. 5 and 6; Rego et al., 2021), a lower fraction of dissolved Fe-carbonate_{ankerite} determined from the HAC leachate is expected in this sample. This is supported by our data that show only an average of $42.14 \pm 4.1\%$ ($n = 6$) dissolved Fe-carbonate_{ankerite} based on the Fe content in the leachate. Therefore, the present data suggest that HAC leachates dissolved most (if not all) carbonates, including calcite and Fe-carbonates among the IF, Fe-rich and Fe-poor studied samples.

Samples treated with 0.4 M HCl showed larger mass loss compared to HAC treatments, particularly for IF and Fe-rich carbonate samples. This implies that other mineralogical phases (distinct from carbonates) may have been dissolved. This inference is supported by the slightly heavier $\delta^{56}\text{Fe}$ values observed in the 0.4 M HCl leachates for IF ($+0.20 \pm 0.05$ ‰) and Fe-rich carbonate (-0.67 ± 0.06 ‰) compared to average $\delta^{56}\text{Fe}$ values from HAC leachates (IF, $+0.14 \pm 0.02$ ‰, $n = 6$; Fe-rich carbonate, -0.72 ± 0.02 ‰, $n = 6$; Fig. 7). In this case, partial dissolution of other phases, such as Fe-oxides which are often enriched in ^{56}Fe compared to Fe-carbonates (Friedrich et al., 2014, 2019; Johnson et al., 2008b; Wiesli et al., 2004) may have contributed to a heavier isotopic composition in the HCl treatments. In contrast, iron-poor carbonates treated with 0.4 M HCl showed slightly lower $\delta^{56}\text{Fe}$ value compared to HAC treatments possibly reflecting partial dissolution of a depleted ^{56}Fe source. Pyrite is abundant in this Fe-poor carbonate sample and represents a potential contributor to the dissolved iron pool (Fig. 5C; Rego et al., 2021). An important conclusion is that, despite a small difference in Fe isotope composition between HCl and HAC treatments, the values are relatively similar considering analytical error and isotopic variability between different samples (Table 3, Fig. 7).

Importantly, no analytical artefact was observed related to carbonate dissolution utilizing 5, 10 or 20% HAC treatments as illustrated with the lack correlation between the amount of Fe-carbonate dissolved and its $\delta^{56}\text{Fe}$ values (Fig. 8). A previous study observed anomalous Fe isotope fractionation related to dissolution of magnetite with 20% HAC (Hyslop et al., 2008), however, von Blanckenburg et al. (2008) were not able to reproduce such anomalies. Additionally, we performed similar dissolution tests with HAC (5% and 10%) in pure magnetite grains of variable sizes (Fig. 2), and the results support previous findings in which only very low Fe content was measured in the leachate (i.e. $< 1\%$ Fe, Table 4) after treatment (von Blanckenburg et al., 2008).

To summarize, the differences in HAC concentrations (5, 10, and 20%) do not change the amount of mass loss variation, the fraction of Fe-carbonate being dissolved, and the iron isotope composition of IF, Fe-rich and Fe-poor carbonate leachates, at least when using the present protocol (i.e. room temperature, reaction time of 12 h). Weak HAC dissolution is shown to achieve complete dissolution of carbonates in IF, Fe-rich and Fe-poor carbonate samples. Dissolution tests with 0.4 M

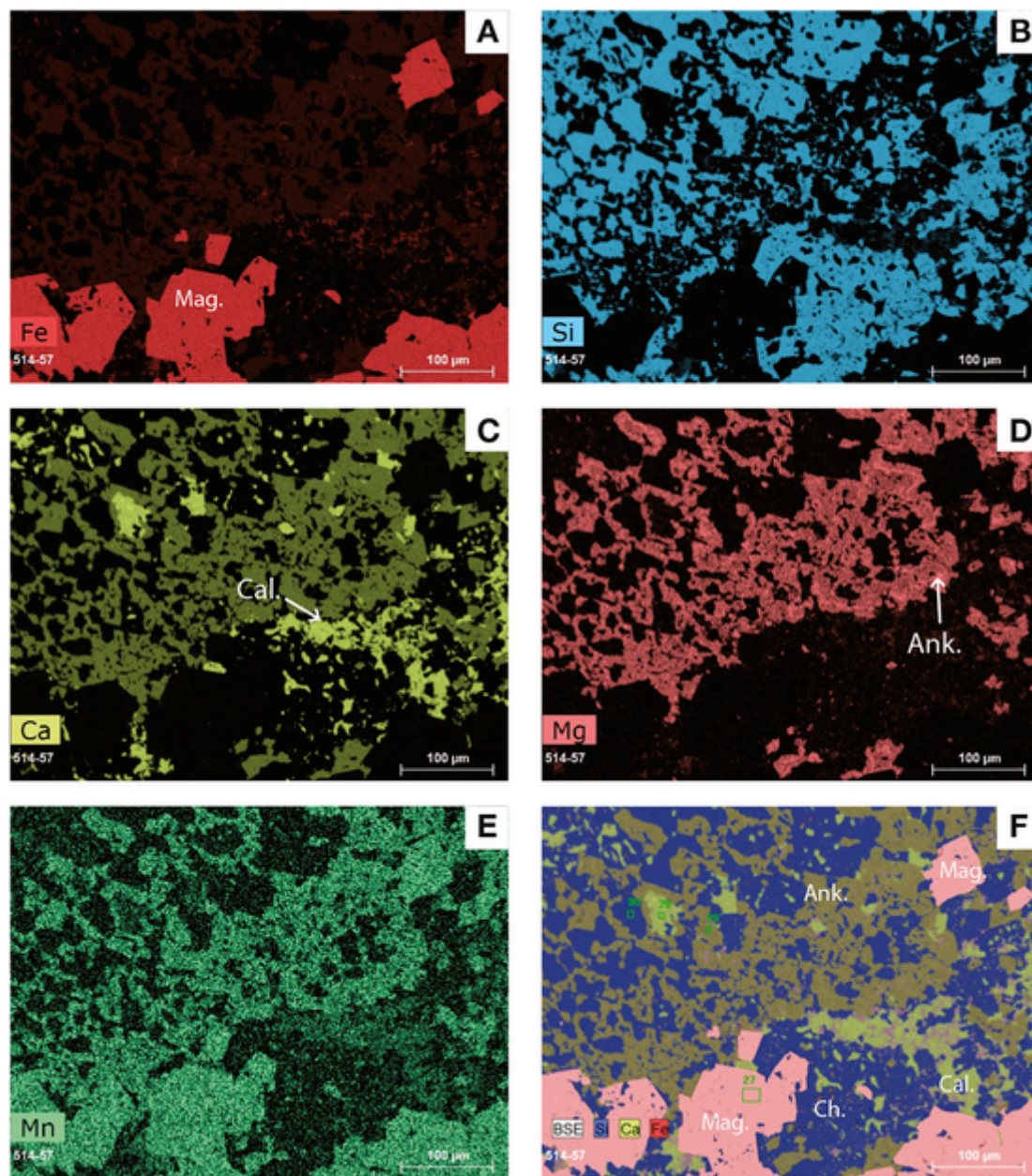


Fig. 6. Elemental map done by scanning electron microscopy (SEM) showing (A) Fe, (B) Si, (C) Ca, (D) Mg, (E) Mn, and (F) a composite showing the occurrence ankerite and calcite together in the Fe-poor carbonate sample.

HCl demonstrate higher mass loss compared to carbonate content, thus likely reflecting partial dissolution of other mineralogical phases (e.g. Fe-oxides, Fe-sulfides). Previous studies have shown that weak HAC attacks can dissolve most ankerite (93.6% fraction of Fe in leachate) (von Blanckenburg et al., 2008), and even though only partial digestion of siderite is attained with 5 to 10% HAC (e.g. Rongemaille et al., 2011; this study), we show here that its iron isotope composition is preserved without generating anomalous results. Accordingly, when targeting Fe isotope composition of carbonate minerals in Archean IF and Fe-carbonates samples, weak HAC should be preferentially used to avoid dissolution of other mineralogical phases. This method could represent an alternative to other mineral-specific extraction protocols (e.g. Poulton and Canfield, 2005; Henkel et al., 2016) and to in-situ measurements, and providing key insights into isotopic fractionation associated to Fe-carbonate formation processes and Fe biogeochemical cycle in the Precambrian ocean.

4.3. Implications for paleo-environment reconstructions

By measuring the Fe isotope composition of carbonates, we can obtain insights into mineral formation processes, which could be related to either mineral precipitating from a primary seawater component or result from early to late diagenetic transformations (e.g. Johnson et al., 2013). The $\delta^{56}\text{Fe}$ values of Fe-carbonates extracted from IF, Fe-rich, and Fe-poor carbonates in Carajás Formation are $+0.14 \pm 0.02\text{‰}$ ($n = 6$), $-0.74 \pm 0.02\text{‰}$ ($n = 6$), and $-0.15 \pm 0.01\text{‰}$ ($n = 6$), respectively. Given that dissolved Fe(II) was hydrothermally sourced to the Carajás Basin (e.g. Rego et al., 2021) with similar isotopic composition of modern hydrothermal fluids ($-0.5 < \delta^{56}\text{Fe}_{\text{hydrothermal fluid}} < +0.1$; Sharma et al., 2001; Beard et al., 2003; Johnson et al., 2008a; Bennett et al., 2009; Rouxel et al., 2016), Fe-carbonates (i.e. siderite) forming in equilibrium with Archean seawater are expected to have $\delta^{56}\text{Fe}$ values between ~ -0.26 to -0.70‰ as determined experimentally (Wiesli et al., 2004). Therefore, iron-rich carbonate (ankerite dominated) with $\delta^{56}\text{Fe}$

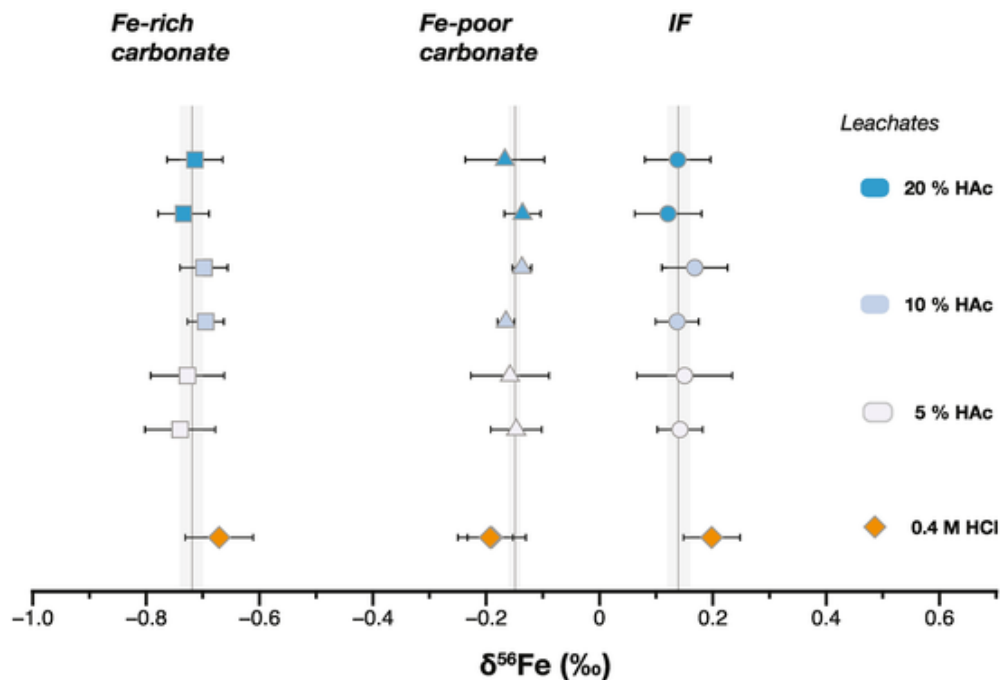


Fig. 7. Iron isotope ($\delta^{56}\text{Fe}$) composition of leachates using acetic acid (HAc 5%, 10% and 20%) and 0.4 M HCl from three natural samples, including an iron formation, Fe-rich and Fe-poor carbonate.

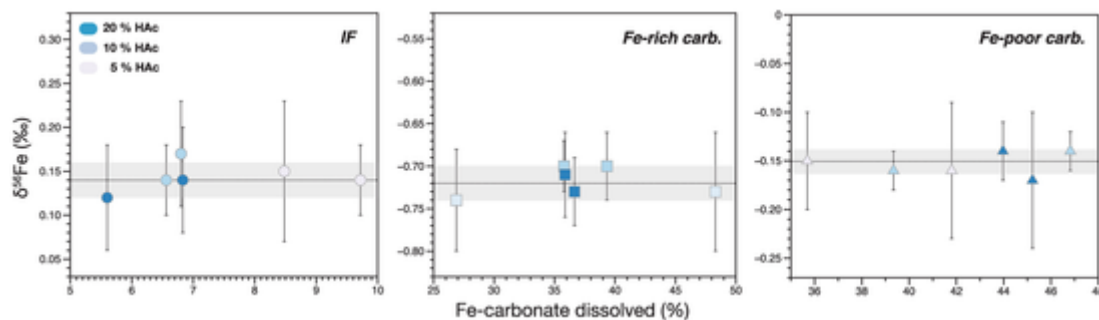


Fig. 8. Iron isotope ($\delta^{56}\text{Fe}$) composition of leachates using acetic acid (HAc 5%, 10% and 20%) from three natural samples (iron formation, Fe-rich and Fe-poor carbonate) and its relation to the amount of Fe-carbonate dissolved after each treatment. Analytical errors for each measurement is reported with error bars as 2 standard-deviation, while dashed line represents the average $\delta^{56}\text{Fe}$ value among all HAc treatments and gray-shaded area represents the 1 standard-deviation.

values of $-0.74 \pm 0.02\text{‰}$ ($n = 6$) is consistent with a precipitation in equilibrium with Carajás' paleoseawater. Similarly, this could be the case for the Fe-poor carbonate with abundant calcite in its composition as shown by petrographic observations (Figs. 5 and 6, Rego et al., 2021). In this sample, there is likely a higher contribution from Fe incorporated into calcite grains, thus reflecting a hydrothermal fluid-like composition as shown with heavier $\delta^{56}\text{Fe}$ values (e.g. $-0.15 \pm 0.01\text{‰}$, $n = 6$) compared to the Fe-rich carbonate sample. This suggests that carbonates from Fe-rich and Fe-poor samples could have formed in equilibrium with seawater, and hence be a proxy for past seawater conditions. Equivalent light $\delta^{56}\text{Fe}$ values were observed in platform carbonates from the Hamersley Basin, Australia, (e.g. Wittenoon Dolomite; Craddock and Dauphas, 2011a) and the Transvaal Basin, South Africa (e.g. Gamohaam Formation; Heimann et al., 2010).

In contrast, the positive $\delta^{56}\text{Fe}$ values measured in Fe-carbonates from IF ($+0.14 \pm 0.02\text{‰}$, $n = 6$) are unlikely to be reflecting precipitation in isotopic equilibrium with Archean seawater, as demonstrated experimentally and theoretically (Anbar et al., 2005; Blanchard et al., 2009; Schauble et al., 2001; Wiesli et al., 2004). Iron-carbonates with a positive $\delta^{56}\text{Fe}$ value can be explained by ankerite and/or siderite precipitating from a pool of $\text{Fe(II)}_{\text{aq}}$ enriched in ^{56}Fe (Heimann et al., 2010; Craddock and Dauphas, 2011a). Different degrees of partial oxidation

favoured by photoferrotophths likely induced the formation of Fe-oxides with positive $\delta^{56}\text{Fe}$ values in the Carajás Basin (Rego et al., 2021). An efficient reductive dissolution of Fe-oxides by microbial respiration (i.e. dissimilatory iron reduction, DIR) could explain an authigenic Fe(II) reservoir enriched in ^{56}Fe in sediment pore space where carbonates were likely precipitating from (Craddock and Dauphas, 2011a; Johnson et al., 2013). This DIR model supports the positive $\delta^{56}\text{Fe}$ values measured in carbonates from IFs and are in agreement with previous studies that also invoked microbial respiration as a mechanism favoring carbonate precipitation in pore water particularly within Fe-rich and IF samples (Craddock and Dauphas, 2011a; Heimann et al., 2010; Johnson et al., 2008a, 2013; Tong et al., 2021). Moreover, the lower content of total organic carbon (TOC) measured in IF samples compared to the Fe-rich and Fe-poor carbonate samples (e.g. Rego et al., 2021) supports oxidation of organic carbon coupled to the reduction of Fe(III) as a product of DIR. Collectively, Fe-carbonates from IF reflect microbial processes in sediment pore space (i.e. early diagenesis), whereas Fe-rich and Fe-poor carbonates record shallow seawater chemistry and surface-environmental conditions. Distinguishing between different Fe isotope signatures among carbonates provides constrain on the Fe biogeochemical cycle during the Neoproterozoic, and shows that similar mechanism (e.g. microbial DIR) described from the geological record elsewhere

(Australia and South Africa) was also operating in Carajás, Brazil ~2.74 Gyr ago.

5. Conclusions and perspectives

We measured the Fe isotope composition of Fe-carbonate phases extracted by weak acetic acid leaching protocols. A series of tests with distinct acids (e.g. HAc and HCl) at different concentrations performed on Fe-carbonate standard (i.e. siderite) and natural samples common in the Precambrian (i.e. iron formations and Fe-rich and -poor carbonates) have shown that partial and/or total dissolution may occur depending on the Fe-carbonate mineral being dissolved. Partial dissolution of siderite (~13 to 60%) was observed using 5 to 20% acetic acid for 12 h at room temperature. However, the Fe isotope composition of the partially dissolved leachate fraction was undistinguishable from the values measured for a total siderite dissolution (i.e. utilizing HCl for longer reaction times, or concentrated HCl-HNO₃ solution). Moreover, the same protocol achieved mostly complete dissolution of Fe-carbonates and carbonate (ankerite and calcite) from natural samples, while 0.4 M HCl attacks was potentially dissolving other mineralogical phases.

We therefore recommend the utilization of 5 to 10% HAc digestions to target Fe-carbonates in natural samples, particularly those dominated by ankerite and calcite, to finally avoid substantial dissolution of other mineral phases. In the case of siderite-rich samples, we noticed that ~30% dissolution of a pure siderite standard still preserves the Fe isotope composition of its whole rock value. However, in the case of sequential extraction, one should have in mind that part of the siderite may remain in the residue and be cumulated to the next extraction stages. Therefore, studies focusing on sequential extractions are recommended to follow previously published methods (e.g. PC method) which yields ~100% dissolution of siderite. Despite other sequential extraction methods proven to be efficient (Poulton and Canfield, 2005), our acetic acid leaching protocol is less laborious/arduous and could be an alternative option to effectively target Fe-carbonates particularly for Fe isotopic studies trying to reconstruct ancient Fe cycling on Earth and elsewhere based on Fe-bearing minerals.

Uncited reference

Nie et al., 2020

Declaration of Competing Interest

The authors declare that they have no known competing financial interests or personal relationships that could have appeared to influence the work reported in this paper.

Data availability

All data presented here can be found in the main text.

Acknowledgements

This research was funded by Fundação de Amparo à Pesquisa do Estado de São Paulo, FAPESP (2019/16271-0; 2018/05892-0; 2015/16235-2;). We thank Pierre Burckel for his technical assistance during ICP-AES analyses. N. X. Nie and an anonymous reviewer are thanked for the comments and suggestions that greatly improved the manuscript. V. B. thanks the Institut Universitaire de France for funding (IUF#2017-2021). Parts of this work were supported by IPGP multidisciplinary program PARI and by Paris-IdF region SESAME, under Grant no. 12015908.

References

- Anbar, A.D., Jarzecki, A.A., Spiro, T.G., 2005. Theoretical investigation of iron isotope fractionation between Fe(H₂O)₆³⁺ and Fe(H₂O)₆²⁺: implications for iron stable isotope geochemistry. *Geochim. Cosmochim. Acta* 69, 825–837. <https://doi.org/10.1016/j.gca.2004.06.012>.
- Bayon, G., German, C.R., Boella, R.M., Milton, J.A., Taylor, R.N., Nesbitt, R.W., 2002. An improved method for extracting marine sediment fractions and its application to Sr and Nd isotopic analysis. *Chem. Geol.* 187, 179–199. [https://doi.org/10.1016/S0009-2541\(01\)00416-8](https://doi.org/10.1016/S0009-2541(01)00416-8).
- Beard, B.L., Johnson, C.M., Skulan, J.L., Nealson, K.H., Cox, L., Sun, H., 2003. Application of Fe isotopes to tracing the geochemical and biological cycling of Fe. *Chem. Geol.* 195, 87–117. [https://doi.org/10.1016/S0009-2541\(02\)00390-X](https://doi.org/10.1016/S0009-2541(02)00390-X).
- Becker, R.H., Clayton, R.N., 1972. Carbon isotopic evidence for the origin of a banded iron-formation in Western Australia. *Geochim. Cosmochim. Acta* 36, 577–595. [https://doi.org/10.1016/0016-7037\(72\)90077-4](https://doi.org/10.1016/0016-7037(72)90077-4).
- Bennett, S.A., Rouxel, O., Schmidt, K., Garbe-Schönberg, D., Statham, P.J., German, C.R., 2009. Iron isotope fractionation in a buoyant hydrothermal plume, 5°S Mid-Atlantic Ridge. *Geochim. Cosmochim. Acta* 73, 5619–5634. <https://doi.org/10.1016/j.gca.2009.06.027>.
- Beukes, N.J., Klein, C., 1990. Geochemistry and sedimentology of a facies transition - from microbanded to granular iron-formation - in the early Proterozoic Transvaal Supergroup, South Africa. *Precambrian Res.* 47, 99–139. [https://doi.org/10.1016/0301-9268\(90\)90033-M](https://doi.org/10.1016/0301-9268(90)90033-M).
- Beukes, N.J., Klein, C., Kaufman, A.J., Hayes, J.M., 1990. Carbonate petrography, kerogen distribution, and carbon and oxygen isotope variations in an early proterozoic transition from limestone to iron-formation deposition, transvaal supergroup, South Africa. *Econ. Geol.* 85, 663–690.
- Blanchard, M., Poirasson, F., Méheut, M., Lazzari, M., Mauri, F., Balan, E., 2009. Iron isotope fractionation between pyrite (FeS₂), hematite (Fe₂O₃) and siderite (FeCO₃): a first-principles density functional theory study. *Geochim. Cosmochim. Acta* 73, 6565–6578. <https://doi.org/10.1016/j.gca.2009.07.034>.
- Busigny, V., Lebeau, O., Ader, M., Krapež, B., Bekker, A., 2013. Nitrogen cycle in the Late Archean ferruginous ocean. *Chem. Geol.* 362, 115–130. <https://doi.org/10.1016/j.chemgeo.2013.06.023>.
- Busigny, V., Planavsky, N.J., Jézéquel, D., Crowe, S., Louvat, P., Moureau, J., Viollier, E., Lyons, T.W., 2014. Iron isotopes in an Archean Ocean analogue. *Geochim. Cosmochim. Acta* 133, 443–462. <https://doi.org/10.1016/j.gca.2014.03.004>.
- Busigny, V., Marin-Carbone, J., Muller, E., Cartigny, P., Rollion-Bard, C., Assayag, N., Philippot, P., 2017. Iron and sulfur isotope constraints on redox conditions associated with the 3.2 Ga barite deposits of the Mapepe Formation (Barberton Greenstone Belt, South Africa). *Geochim. Cosmochim. Acta* 210, 247–266. <https://doi.org/10.1016/j.gca.2017.05.002>.
- Busigny, V., Planavsky, N.J., Goldbaum, E., Lechte, M.A., Feng, L., Lyons, T.W., 2018. Origin of the Neoproterozoic Fulu iron formation, South China: insights from iron isotopes and rare earth element patterns. *Geochim. Cosmochim. Acta* 242, 123–142. <https://doi.org/10.1016/j.gca.2018.09.006>.
- Chapman, J.B., Weiss, D.J., Shan, Y., Lemburger, M., 2009. Iron isotope fractionation during leaching of granite and basalt by hydrochloric and oxalic acids. *Geochim. Cosmochim. Acta* 73, 1312–1324. <https://doi.org/10.1016/j.gca.2008.11.037>.
- Craddock, P.R., Dauphas, N., 2011a. Iron and carbon isotope evidence for microbial iron respiration throughout the Archean. *Earth Planet. Sci. Lett.* 303, 121–132. <https://doi.org/10.1016/j.epsl.2010.12.045>.
- Craddock, P.R., Dauphas, N., 2011b. Iron isotopic compositions of geological reference materials and chondrites. *Geostand. Geoanal. Res.* 35, 101–123. <https://doi.org/10.1111/j.1751-908X.2010.00085.x>.
- Dauphas, N., Janney, P.E., Mendybaev, R.A., Wadhwa, M., Richter, F.M., Davis, A.M., Van Zuilen, M., Hines, R., Foley, C.N., 2004. Hromatographic separation and multicollection-ICPMS analysis of iron. Investigating mass-dependent and -independent isotope effects. *Anal. Chem.* 76, 5855–5863. <https://doi.org/10.1021/ac0497095>.
- Dauphas, N., Pourmand, A., Teng, F.Z., 2009. Routine isotopic analysis of iron by HR-MC-ICPMS: how precise and how accurate? *Chem. Geol.* 267, 175–184. <https://doi.org/10.1016/j.chemgeo.2008.12.011>.
- Fischer, W.W., Schroeder, S., Lacassie, J.P., Beukes, N.J., Goldberg, T., Strauss, H., Horstmann, U.E., Schrag, D.P., Knoll, A.H., 2009. Isotopic constraints on the Late Archean carbon cycle from the Transvaal Supergroup along the western margin of the Kaapvaal Craton, South Africa. *Precambrian Res.* 169, 15–27. <https://doi.org/10.1016/j.precamres.2008.10.010>.
- Frierdich, A.J., Beard, B.L., Reddy, T.R., Scherer, M.M., Johnson, C.M., 2014. Iron isotope fractionation between aqueous Fe(II) and goethite revisited: New insights based on a multi-direction approach to equilibrium and isotopic exchange rate modification. *Geochim. Cosmochim. Acta* 139, 383–398. <https://doi.org/10.1016/j.gca.2014.05.001>.
- Frierdich, A.J., Nebel, O., Beard, B.L., Johnson, C.M., 2019. Iron isotope exchange and fractionation between hematite (α-Fe₂O₃) and aqueous Fe(II): a combined three-isotope and reversal-approach to equilibrium study. *Geochim. Cosmochim. Acta* 245, 207–221. <https://doi.org/10.1016/j.gca.2018.10.033>.
- Frost, C.D., von Blanckenburg, F., Schoenberg, R., Frost, B.R., Swapp, S.M., 2007. Preservation of Fe isotope heterogeneities during diagenesis and metamorphism of banded iron formation. *Contrib. Mineral. Petrol.* 153, 211–235. <https://doi.org/10.1007/s00410-006-0141-0>.
- García, A.K., Cavanaugh, C.M., Kacar, B., 2021. The curious consistency of carbon biosignatures over billions of years of Earth-life coevolution. *ISME J.* 15, 2183–2194. <https://doi.org/10.1038/s41396-021-00971-5>.

- Havas, R., Savian, J.F., Busigny, V., 2021. Iron isotope signature of magnetofossils and oceanic biogeochemical changes through the Middle Eocene Climatic Optimum. *Geochim. Cosmochim. Acta* 311, 332–352. <https://doi.org/10.1016/j.gca.2021.07.007>.
- Heimann, A., Johnson, C.M., Beard, B.L., Valley, J.W., Roden, E.E., Spicuzza, M.J., Beukes, N.J., 2010. Fe, C, and O isotope compositions of banded iron formation carbonates demonstrate a major role for dissimilatory iron reduction in ~2.5Ga marine environments. *Earth Planet. Sci. Lett.* 294, 8–18. <https://doi.org/10.1016/j.epsl.2010.02.015>.
- Henkel, S., Kasten, S., Poulton, S.W., Staubwasser, M., 2016. Determination of the stable iron isotopic composition of sequentially leached iron phases in marine sediments. *Chem. Geol.* 421, 93–102. <https://doi.org/10.1016/j.chemgeo.2015.12.003>.
- Holland, H.D., 1984. *The Chemical Evolution of the Atmosphere and Oceans*. Princeton University Press, Princeton.
- Holland, H.D., 2002. Volcanic gases, black smokers, and the Great Oxidation Event. *Geochim. Cosmochim. Acta* 66, 3811–3826. <https://doi.org/10.1016/j.gca.2002.01.029>.
- Hyslop, E.V., Valley, J.W., Johnson, C.M., Beard, B.L., 2008. The effects of metamorphism on O and Fe isotope compositions in the Biwabik Iron Formation, northern Minnesota. *Contrib. Mineral. Petrol.* 155, 313–328. <https://doi.org/10.1007/s00410-007-0244-2>.
- James, H.L., 1954. Sedimentary facies of iron-formation. *Econ. Geol.* 49, 235–293.
- Jiang, C.Z., Tosca, N.J., 2019. Fe(II)-carbonate precipitation kinetics and the chemistry of anoxic ferruginous seawater. *Earth Planet. Sci. Lett.* 506, 231–242. <https://doi.org/10.1016/j.epsl.2018.11.010>.
- Jiang, C.Z., Halevy, I., Tosca, N.J., 2022. Kinetic isotope effect in siderite growth: implications for the origin of banded iron formation siderite. *Geochim. Cosmochim. Acta* 322, 260–273. <https://doi.org/10.1016/j.gca.2022.01.029>.
- Johnson, C.M., Beard, B.L., Klein, C., Beukes, N.J., Roden, E.E., 2008a. Iron isotopes constrain biologic and abiologic processes in banded iron formation genesis. *Geochim. Cosmochim. Acta* 72, 151–169. <https://doi.org/10.1016/j.gca.2007.10.013>.
- Johnson, C.M., Beard, B.L., Roden, E.E., 2008b. The iron isotope fingerprints of redox and biogeochemical cycling in modern and ancient Earth. *Annu. Rev. Earth Planet. Sci.* 36, 457–493. <https://doi.org/10.1146/annurev.earth.36.031207.124139>.
- Johnson, C.M., Ludois, J.M., Beard, B.L., Beukes, N.J., Heimann, A., 2013. Iron formation carbonates: paleoceanographic proxy or recorder of microbial diagenesis? *Geology* 41, 1147–1150. <https://doi.org/10.1130/G34698.1>.
- Justo, A.P., Dantas, E.L., Bau, M., Freitas-Silva, F.H., Santos, R.V., Schorscher, J.H.D., 2020. Paleobasinal to band-scale REE + Y distribution in iron formations from Carajás, Amazon Craton, Brazil. *Ore Geol. Rev.* 127, 103750. <https://doi.org/10.1016/j.oregeorev.2020.103750>.
- Kaufman, A.J., Hayes, J.M., Klein, C., 1990. Primary and diagenetic controls of isotopic compositions of iron-formation carbonates. *Geochim. Cosmochim. Acta* 54, 3461–3473. [https://doi.org/10.1016/0016-7037\(90\)90298-Y](https://doi.org/10.1016/0016-7037(90)90298-Y).
- Kaufman, A.J., Hayes, J.M., Knoll, A.H., Germs, G.J.B., 1991. Isotopic compositions of carbonates and organic carbon from upper Proterozoic successions in Namibia: stratigraphic variation and the effects of diagenesis and metamorphism. *Precambrian Res.* 49, 301–327. [https://doi.org/10.1016/0301-9268\(91\)90039-D](https://doi.org/10.1016/0301-9268(91)90039-D).
- Klein, C., 2005. Some Precambrian banded iron-formations (BIFs) from around the world: their age, geologic setting, mineralogy, metamorphism, geochemistry, and origin. *Am. Mineral.* 90, 1473–1499. <https://doi.org/10.2138/am.2005.1871>.
- Klein, C., Beukes, N.J., 1989. Geochemistry and sedimentology of a facies transition — from limestone to iron-formation deposition in the early Proterozoic Transvaal Supergroup, South Africa. *Econ. Geol.* 84, 1733–1774.
- Konhauser, K.O., Newman, D.K., Kappler, A., 2005. The potential significance of microbial Fe(III) reduction during deposition of Precambrian banded iron formations. *Geobiology* 3, 167–177.
- Konhauser, K.O., Planavsky, N.J., Hardisty, D.S., Robbins, L.J., Warchola, T.J., Haugaard, R., Lalonde, S.V., Partin, C.A., Oonk, P.B.H., Tsikos, H., Lyons, T.W., Bekker, A., Johnson, C.M., 2017. Iron formations: a global record of Neoproterozoic to Palaeoproterozoic environmental history. *Earth-Sci. Rev.* 172, 140–177. <https://doi.org/10.1016/j.earscirev.2017.06.012>.
- Lebeau, O., Busigny, V., Chaduteau, C., Ader, M., 2014. Organic matter removal for the analysis of carbon and oxygen isotope compositions of siderite. *Chem. Geol.* 372, 54–61. <https://doi.org/10.1016/j.chemgeo.2014.02.020>.
- Marin-Carbonne, J., Busigny, V., Miot, J., Rollion-Bard, C., Muller, E., Drabon, N., Jacob, D., Pont, S., Robyr, M., Bontognali, T.R.R., François, C., Reynaud, S., Van Zuilen, M., Philippot, P., 2020. In situ Fe and S isotope analyses in pyrite from the 3.2 Ga Mendon Formation (Barberton Greenstone Belt, South Africa): evidence for early microbial iron reduction. *Geobiology* 1–20. <https://doi.org/10.1111/gbi.12385>.
- McCoy, V.E., Asael, D., Planavsky, N., 2017. Benthic iron cycling in a high-oxygen environment: Implications for interpreting the Archean sedimentary iron isotope record. *Geobiology* 15, 619–627. <https://doi.org/10.1111/gbi.12247>.
- Nie, N.X., Dauphas, N., Villalon, K.L., Liu, N., Heard, A.W., Morris, R.V., Mertzman, S.A., 2020. Iron isotopic and chemical tracing of basalt alteration and hematite spherule formation in Hawaii: a prospective study for Mars. *Earth Planet. Sci. Lett.* 544, 116385. <https://doi.org/10.1016/j.epsl.2020.116385>.
- Oonk, P.B.H., Tsikos, H., Mason, P.R.D., Henkel, S., Staubwasser, M., Fryer, L., Poulton, S.W., Williams, H.M., 2017. Fraction-specific controls on the trace element distribution in iron formations: Implications for trace metal stable isotope proxies. *Chem. Geol.* 474, 17–32. <https://doi.org/10.1016/j.chemgeo.2017.10.018>.
- Poulton, S.W., Canfield, D.E., 2005. Development of a sequential extraction procedure for iron: implications for iron partitioning in continentally derived particulates. *Chem. Geol.* 214, 209–221. <https://doi.org/10.1016/j.chemgeo.2004.09.003>.
- Raiswell, R., Canfield, D.E., 2012. The iron biogeochemical cycle past and present. *Geochim. Perspect.* 1, 1–232. <https://doi.org/10.7185/geochempersp.1.1>.
- Rego, E.S., Busigny, V., Lalonde, S.V., Philippot, P., Bouyon, A., Rossignol, C., Babinski, M., Cássia Zapparoli, A., 2021. Anoxygenic photosynthesis linked to Neoproterozoic iron formations in Carajás (Brazil). *Geobiology* 19, 326–341. <https://doi.org/10.1111/gbi.12438>.
- Rongemaille, E., Bayon, G., Pierre, C., Bollinger, C., Chu, N.C., Fouquet, Y., Riboulot, V., Voisset, M., 2011. Rare earth elements in cold seep carbonates from the Niger delta. *Chem. Geol.* 286, 196–206. <https://doi.org/10.1016/j.chemgeo.2011.05.001>.
- Rosenbaum, J., Sheppard, S.M.F., 1986. An isotopic study of siderites dolomites and ankerites at high temperatures. *Geochim. Cosmochim. Acta* 50, 1147–1150.
- Rouxel, O., Dobbek, N., Ludden, J., Fouquet, Y., 2003. Iron isotope fractionation during oceanic crust alteration. *Chem. Geol.* 202, 155–182. <https://doi.org/10.1016/j.chemgeo.2003.08.011>.
- Rouxel, O., Toner, B.M., Mangani, S.J., German, C.R., 2016. Geochemistry and iron isotope systematics of hydrothermal plume fall-out at East Pacific rise 9°50'N. *Chem. Geol.* 441, 212–234. <https://doi.org/10.1016/j.chemgeo.2016.08.027>.
- Schauble, E.A., Rossman, G.R., Taylor, H.P., 2001. Theoretical estimates of equilibrium Fe-isotope fractionations from vibrational spectroscopy. *Geochim. Cosmochim. Acta* 65, 2487–2497. [https://doi.org/10.1016/S0016-7037\(01\)00600-7](https://doi.org/10.1016/S0016-7037(01)00600-7).
- Sharma, M., Polizzotto, M., Anbar, A.D., 2001. Iron isotopes in hot springs along the Juan de Fuca Ridge. *Earth Planet. Sci. Lett.* 194, 39–51. [https://doi.org/10.1016/S0012-821X\(01\)00538-6](https://doi.org/10.1016/S0012-821X(01)00538-6).
- Slotznick, S.P., Eiler, J.M., Fischer, W.W., 2018. The effects of metamorphism on iron mineralogy and the iron speciation redox proxy. *Geochim. Cosmochim. Acta* 224, 96–115. <https://doi.org/10.1016/j.gca.2017.12.003>.
- Steinboeckel, G., Von Blanckenburg, F., Horn, I., Konhauser, K.O., Beukes, N.J., Gutzmer, J., 2010. Deciphering formation processes of banded iron formations from the Transvaal and the Hamersley successions by combined Si and Fe isotope analysis using UV femtosecond laser ablation. *Geochim. Cosmochim. Acta* 74, 2677–2696. <https://doi.org/10.1016/j.gca.2010.01.028>.
- Taylor, P.D.P., Maeck, R., De Bièvre, P., 1992. Determination of the absolute isotopic composition and Atomic Weight of a reference sample of natural iron. *Int. J. Mass Spectrom. Ion Process.* 121, 111–125. [https://doi.org/10.1016/0168-1176\(92\)80075-C](https://doi.org/10.1016/0168-1176(92)80075-C).
- Tong, X., Mänd, K., Li, Y., Zhang, L., Peng, Z., Wu, Q., Li, P., Zhai, M., Robbins, L.J., Wang, C., Konhauser, K.O., 2021. Iron and carbon isotope constraints on the formation pathway of iron-rich carbonates within the dagushan iron formation, North China Craton. *Minerals* 11, 1–20. <https://doi.org/10.3390/min11010094>.
- von Blanckenburg, F., Mamberti, M., Schoenberg, R., Kamber, B.S., Webb, G.E., 2008. The iron isotope composition of microbial carbonate. *Chem. Geol.* 249, 113–128. <https://doi.org/10.1016/j.chemgeo.2007.12.001>.
- Weyer, S., Schwieters, J.B., 2003. High precision Fe isotope measurements with high mass resolution MC-ICPMS. *Int. J. Mass Spectrom.* 226, 355–368. [https://doi.org/10.1016/S1387-3806\(03\)00078-2](https://doi.org/10.1016/S1387-3806(03)00078-2).
- Wiesli, R.A., Beard, B.L., Johnson, C.M., 2004. Experimental determination of Fe isotope fractionation between aqueous Fe(II), siderite and “green rust” in abiotic systems. *Chem. Geol.* 211, 343–362. <https://doi.org/10.1016/j.chemgeo.2004.07.002>.